RSC Advances

ROYAL SOCIETY OF CHEMISTRY

www.rsc.org/advances

RSC Advances

ARTICLE

Architectural design of hierarchically meso-macroporous carbon for microbial fuel cells anode

Received 00th January 20xx,
Accepted 00th January 20xx

DOI: 10.1039/x0xx00000x

www.rsc.org/

Mengmeng Liu,[a,b] Minghua Zhou,*[a,b] Liang Ma,[a,b] Huijia Yang,[a,b] Yingying Zhao[a,b]

Larger surface area and porous structure are crucial factors for MFC anode performance. In this study, we demonstrated a dual-templating strategy for design of 3D hierarchically nanostructure carbon (HN-C) with well-patterned macropores (*ca,* 400nm) and ordered mesorpores (*ca*, 4 nm) decorate the carbon cloth as anode for high power density. The HN-C exhibited higher power density (1034 mW m^{-2}) and COD removal efficiency (92.1%) compared with the macroporous carbon anode MFC, mesoporous carbon anode MFC and carbon cloth anode MFC. The excellent performance of HN-C anode MFC was contributed to the combination of mesopores and macropores, providing both the macropores for the bacteria to clog on and a large specific surface area for facilitating fast substrates and electrons transfer to enhance the bioelectrochemical performance. This architectural design of porous carbon materials might open up a promising anode fabrication method to improve MFC performance.

Introduction

Microbial fuel cell (MFC) is potentially useful energy-generating platform, in which chemical energy is directly converted into electrical energy by the electrocatalytic activity of electroactive bacteria[1]. In the past decade, tremendous advances have been made in MFC performances and MFCs with higher power outputs have recently attracted considerable attention[2-6]. The performance of MFCs was dominated by electroactive bacteria indicated by the intensive biofilm at anodes, so anode material as the medium of electron transfer is an essential factor that affects the performance of MFC[7].

Commercially available conventional carbon-based anodes such as carbon cloth[8], porous carbon paper[9], carbon felt[10], and carbon nanotube[11] are widely used as anode in recent research studies. However, low total biomass loading of naturally formed biofilms on these electrode surfaces limits further improvement of energy output in MFCs and performance of other Bioelectrochemical Systems (BES). Large surface area of porous carbons usually has been considered as a basic guiding principle for larger current[12, 13]. Ordered mesoporous carbon (pore size 2~50nm) has been reported to show a faster electron transfer rate, high electrocatalytic activity and improved the MFC performance[14]. However, the pore size of mesoporous carbon (Mes-C) was too narrow which limited for a high MFC performance due to the poor inner pore for the transport of substrate and biomass[15,16].

Proper porous carbon structure anodes with high surface areas are favored because the MFC power output is proportional to the amount of bacteria on the electrode and electrochemical reaction surface[17-19]. Recently, three dimensional (3D) macroporous anodes have been developed and more and more studies have focused on increasing the pore size of the anode to increase the bacteria clogging on the interior of the pores such as textiles[15], sponges[5,20], nickel foam[21], carbon fiber[22] and some carbonized plant material[23]. However, the problems associated with these structures lied in low specific surface area, poor conductivity and low charge transfer efficiency which hampered the power output.

These above two facts demonstrate that both large surface area and macroporous structure of anode are crucial for a high MFC performance. This gives great impetus to combine 3D macroporous carbon (DOM-C) with Mes-C to fabricate hierarchically nanostructure carbon (HN-C) for MFC applications. It is expected that this ordered HN-C with unique pore structure would be a promising MFCs anode possessing high power density, attributed to the suitable ionic transport pathway in hierarchical structures and the macropores for bacteria to attach. However, to the best of our knowledge, HN-C has not yet been used for MFC anode in literature.

[a] *Key Laboratory of Pollution Process and Environmental criteria, Ministry of Education, College of Environmental Science and Engineering, Nankai University, Tainjin 30071, China*
[b] *Key Laboratory of Urban Ecology Environmental Remeidation and Pollution Control, College of Environmental Science and Engineering, Nankai, University, Tianjin 30071, China*
†corresponding author. Tel/Fax:+8602266229619.
E-mail Address: zhoumh@nankai.edu.cn(M. Zhou)

The objective of this work was to verify this feasibility of HN-C as a high power density MFC anode. And it confirmed that this HN-C with mesopores and controlled macropores was promising as MFC anode material for high power density, opening an avenue to develop an architectural design of porous carbon materials to improve power density.

Experimental

Preparation of porous carbon

The monodisperse SiO_2 (~400nm) spheres were prepared by emulsifier-free emulsion polymerization[24]. The carbon-silica nanocomposites were fabricated using a self-assembly method according to previous works with slight modifications[25-27]. Typically, 8.0 g of Pluronic $EO_{20}PO_{70}EO_{20}$ copolymer (P123), 10 mL of 30 wt% sucrose precursors, 10.4 mL of pre-hydrolyzed TEOS solution, 4.8 mL of 0.2 M hydrochloric acid and 10 mL of 50 wt% ethanol solution of SiO_2 were added into the solution under stirring vigorously for 1 h at room temperature. Then the mixture was transferred into Petri dishes and dried at 80°C for 4 h, followed at 150 °C for 6 h. The as-prepared monoliths were scraped from the Petri dishes, and then calcined in a tubular furnace at 900°C at a rate of 5 °C min^{-1} for 2 h. The HN-C-silica nanocomposite was immersed into a 30% HF solution for 72 h to remove silica. The HN-C was obtained by thoroughly wash with deionized water and subsequent drying. The carbon material derived from the above mentioned procedure without addition of SiO_2 latex, denoted as Mes-C, was also fabricated Ⅱ (ES Ⅰ*). In addition, the DOM-C materials were synthesized for comparison using the same process using the SiO_2 colloidal crystal template method (ES Ⅱ*).

Electrode preparation and MFC configuration

The working electrode was prepared by pasting the porous carbon dispersed in Nafion solution (5%, DuPont, USA) with a loading of ~5mg cm^{-2}. For comparison the naked carbon cloth (CC) without HN-C and CC with Mes-C and DOM-C were also used as the working electrodes, respectively. A traditional membrane-free single chamber air-cathode MFC (14 mL volume) was assembled as previously described[28]. Various anodes were used to investigate the variation of power density. The cathode was the Pt /C air cathode (0.3 mg cm^{-2}). MFC was inoculated with 20% anaerobic sludge (TEDA Sewage Treatment Plant, Tianjin), and a medium containing sucrose (2 g L^{-1}) and a 50 mM phosphate buffer solution. The experiments were run 3 times for each electrode test. To evaluate the stability of the porous anode, the MFCs were operated nearly 1 month.

Characterizations and analysis

The surface morphologies of the as-prepared porous carbon before incubation were examined by a field emission scanning electron microscope (FESEM, Hitachi, S-4700) and transmission electron microscopy (TEM, Gatan ORIUS™ SC200C-CD). Fourier-transform infrared (FTIR) spectra were obtained with Brucker Tensor 27 (Germany) under ambient conditions. The spectra were obtained in the wave number range 4000 - 1000 cm^{-1}. Nitrogen adsorption-desorption isotherms and the pore size distribution were collected at 77 K using a Quantachrome autosorb-1-MP automated gas sorption system (USA). The Brunanuer Emmett-Teller (BET) and the pore size distribution were calculated by the Barrett-Joyner-Halenda (BJH) method. Specific surface areas of the samples were determined by nitrogen adsorption data in the relative pressure range from 0.05 to 0.3 using the BET equations. Total pore volumes were determined by the amount of gas adsorbed at the relative pressure of 0.99.

The cell voltage across the external circuit and the anode potential were measured every 30 minutes by a digital multi-meter (PISO-813, ICP DAS Co., Ltd.) connected to a personal computer. Polarization curves were obtained by applying a different external resistance (R, from 10000 Ω to 100 Ω) to the circuit. Electrochemical measurements were carried out on CHI660D workstation (CH Instruments, Chenhua, Shanghai, China). These tests were conducted in a three-electrode single-chamber reactor containing a working electrode (7 cm^2 projected area), a platinum wire counter electrode, and a saturated calomel electrode (SCE) reference electrode. Electrochemical activity of the anodic bacteria was measured by cyclic voltammogram (CV) at a scan rate 30 mV s^{-1} and electrochemical impedance spectroscopy (EIS) was conducted using a potential at the open circuit potential (Voc) in a frequency of 0.01 Hz to 100 kHz. Galvanostatic charge / discharge (C/D) analysis was performed on a land cell tester (Land, CT-2001A, China) at a constant current density of 0.1 A g^{-1}.

Results and discussion

The architectural characterization of porous carbon

Fig. 1 shows the SEM and TEM morphology of the template and the resulting porous carbons. It can be seen that SiO_2 particles are spherical with uniform diameter of about 400nm (Fig. 1a). The DOM-C and HN-C possessed uniform macropores with a diameter similar to that of the silica spheres packed in the colloidal crystal template (Fig. 1b and Fig. 1c). The DOM-C, synthesized in the absence of P123, showed well-ordered 3D porous structures with no mesopores on the wall of macropores. The SEM image of Mes –C (Fig. 1d) showed well 2D porous ordered structures. The interior structure of HN-C was further analyzed by TEM, and the mesoporous channels were clearly observed (Fig. 1e and Fig. 1f). The TEM of HN-C showed the hierarchical ordered porous structure (Fig. 1f) and the average diameter of mesopores of 4 nm was observed (Fig. 1e and f) demonstrating that the dual-templating method was successfully fabricated the ordered multimodal porous architecture.

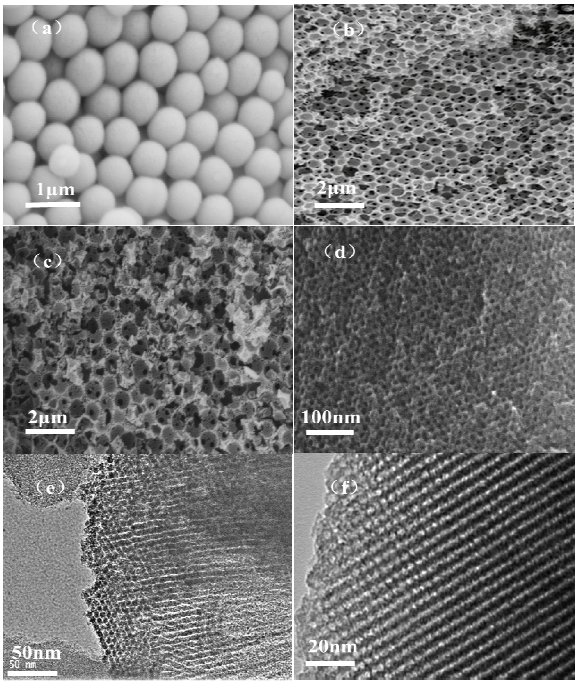

Fig. 1 SEM images of (a) SiO_2 template (b) DOM-C (c) HN-C (d) Mes-C (e,f) TEM of HN-C with different magnifications.

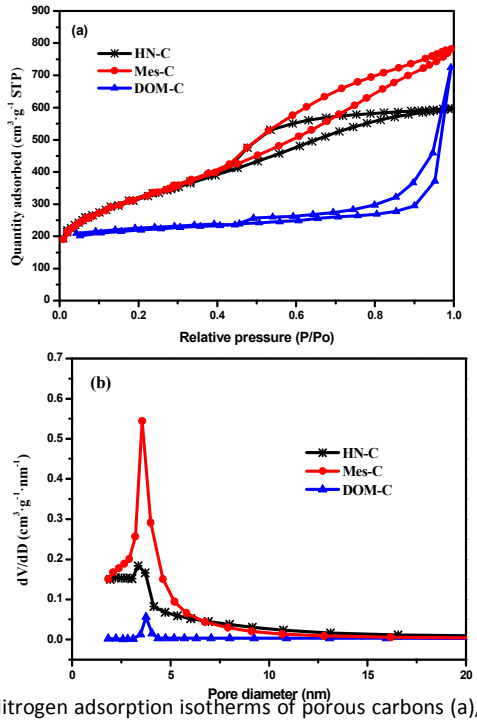

Fig. 2 Nitrogen adsorption isotherms of porous carbons (a), pore size distribution ranged from 0-20 nm (b).

The interior structures of the porous carbon were further analyzed by nitrogen adsorption- desorption isotherms and pore size distributions. As shown in Fig. 2a, the Mes-C, DOM-C and HN-C exhibited typical type IV isotherms with a clear hysteresis loop in the relative pressure (P/P_0) range of 0.45 - 0.8, depicting the mesoporous characteristics. However, the hysteresis loops of three kinds of porous carbon were different. The capillary adsorption of Mes-C at $P/P_0 > 0.4$ was more significant than that of HN-C, indicating a high adsorption volume of Mes-C in the mesoporous region. In addition, a sharp adsorption region at low P/P_0 of 0.0 - 0.1 was clearly observed for all the materials, illustrating the presence of a large amount of micropores. The micropores are ascribed to the emission of small gaseous molecules (e.g. CO_2, H_2, and H_2O).

Table 1. The pore properties of porous carbon materials

Samples	Surface area* ($m^2 g^{-1}$)	Pore volume ($cm^3 g^{-1}$)			
		Total volume	micropore	mesopore	macropores
Mes-C	1207	1.27	0.15	1.12	- -
HN-C	1047.5	1.15	0.21	0.71	0.12
DOM-C	541.1	0.59	0.36	0.10	0.13

Fig. 2b shows the pore size distribution for three porous carbons in the sizes ranged from 0 - 20 nm. The curve of HN-C slightly moved to the small pore size range, but the intensity was higher than that of DOM-C, depicting a large amount of mesopores in HN-C. The three peaks for Mes-C, DOM-C and HN-C that corresponded to 3.61, 3.97, and 3.85 nm indicated that they had a dominant mesoporous structure (Fig. 2b).

The pore structural parameters of porous carbon are listed in Table 1. The specific surface areas of Mes-C and HN-C were 1207.0 and 1047.5 $m^2 g^{-1}$, respectively. It should be noted that the specific surface of DOM-C, derived from the SiO_2 template, was only541.1 $m^2 g^{-1}$, indicating that the surface area of DOM-C was mainly from the meso- and micro-pores. The calculated of pore volume indicated the pore texture of the porous materials. It was clear that the amount of mesopores in Mes-C is larger than DOM-C and the dominating pores for Mes-C were mesopores and no macropores were constructed. The HN-C contained macropores and more mesopores, thus it would exhibit excellent electrochemical performance for the MFC power production. For all of the as-made HN-C carbon, the mesoporous ratios was 54.8 %, further evidencing that these porous carbons was mainly composed of mesopores.

Fig. 3a gives the FTIR spectra of HN-C, Mes-C and DOM-C. The materials were functionalized with hydroxyl and carboxyl groups, which was common for hydrophilic carbon. The peaks at 1520 and 1629 cm^{-1} were the characteristic of -C=C stretching vibration, and the band at 2900 cm^{-1} was due to the -C-H stretching vibration[29]. The bands at 1000 - 1450 cm^{-1} corresponded to C-H stretching and O-H bending vibrations[30].

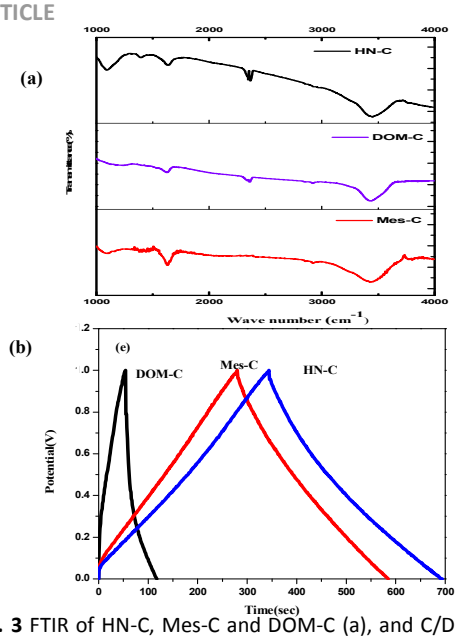

Fig. 3 FTIR of HN-C, Mes-C and DOM-C (a), and C/D behavior of all electrodes (b).

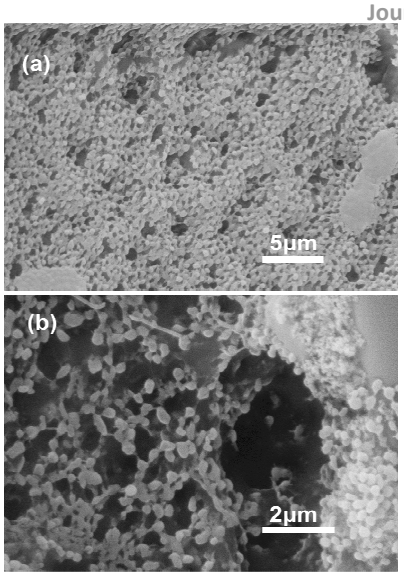

Fig. 4 SEM images of biofilm on the surface (a) and interior (b) of HN-C anode.

The peaks at 1580, 1700 were typically associated with C=O strength[31]. The spectrum of HN-C exhibited increased intensity of the bands at approximately 2350 cm^{-1} and 3000 - 3700 cm^{-1} which were typically associated with C=O strength and the -O-H stretching vibration [30,32], ensuring the hydrophilicity and wettability of as prepared carbonaceous material, which were beneficial to bacterial adherence [33].

The characterization of electrochemical capacitive behavior

The capacitive behavior was studied to investigate the ions transport ability of as-prepared anodes. Previous study revealed that the anodes integrated with internal capacitors improved the performance of MFCs because of the enhanced transient charge storage behavior of the anodes[34]. As shown in Fig. 3b, it was found that the C/D curves of all electrodes were nearly linear and almost symmetrical, demonstrating an excellent reversibility and capacitive property for these electrodes. Both HN-C and Mes-C showed a better performance than DOM-C, attributed to the higher specific surface area and interconnected mesoporous channels in the macroporous walls to form a double-layer capacitance for ions transport. Comparing with the Mes-C, capacitive performance on the HN-C anode was further improved by introducing the macropores due to the reduction of the diffusion length from bulk electrolytes to meso- and micro-porous surfaces [35]. The results demonstrated both the mesopores and macropores played important roles in the ions transport.

Growth of bacteria biofilm on anode

Fig. 4a and Fig. 4b demonstrate the biofilm growth on the surface and interior of HN-C anode. It can be seen that the bacteria have their size of less than 200nm and the bacterial cellsheavily aggregated on the surface (Fig. 4a) and interior of the material in the pores of HN-C (Fig. 4b). As shown in Fig. 4b, lots of small pores observed on the wall of the macropore were mesopores produced by the P123 templates. The result confirmed that the internal macroporosity of HN-C played a crucial role in efficient exploitation of the available surface area. Furthermore, with sufficient spacing in the pores, the biofilm could be formed without completely clogging the macropores, thus favoring mass transport and bacteria infiltration into the interior of the anode. Though the biofilm could also be formed on the bare carbon cloth electrode, it was hard to observe as shown in Fig. S1 because the number of the bacteria on the carbon cloth was far scarcer than the HN-C anode.

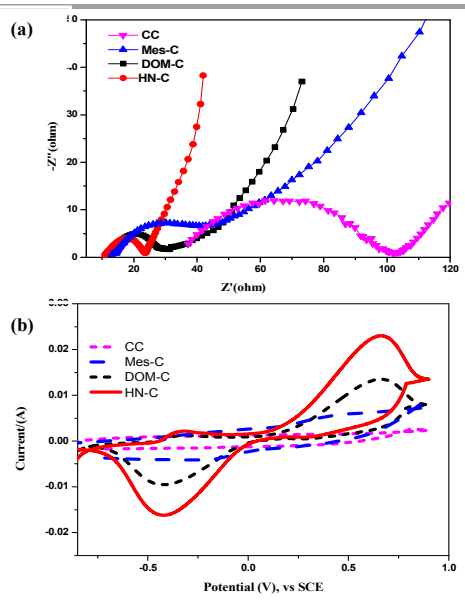

Fig. 5 EIS of MFCs with different biofilm anodes(a);CVs of bacteria on different anodes in a PBS solution (50 mM, pH 7.0) after inoculation for 72 h(b).

To better understand the interaction between biofilm and electrode surface for the overall anode performance, EIS experiments were conducted for all the anodes at the open circuit (Fig. 5a). The CC anode had a largest in the ohmic resistance (66Ω) compared with other anodes based on the same electrolyte indicating the poor biofilm formation due to the lowest surface area for bacteria attachment. Much lower charge transfer resistance from HN-C (13 Ω) was obtained whereas that of Mes-C anode and DOM-C anode after electroactive biofilm formation was 31 Ω and 19 Ω. A lower charge-transfer resistance demonstrated a faster extracellular electron transfer (EET) of the biofilm on the anode surface [36]. The results indicated that the meso-macroporous structure improved the bacterial attachment and electrolyte accessibility.

To accurately identify the biocatalytic active sites responsible for electricity generation, the biofilms were analyzed using CV (Fig. 5b) under the non-turnover condition. The current response increased after the biofilm formed comparing with the naked electrodes in which no peaks were observed (Fig. S2). As shown in Fig. 5b, the HN-C and DOM-C anode showed the redox peak at the potential of -0.38 V vs SCE, which was assigned to the outer membrane c-type *cytochrome* Z (OmcZ) that were vital to the EET in MFCs [37]. In comparison, no obvious redox peaks were found in the Mes-C anode and CC anode. The redox peak current reflected the amount of the redox active species in the biofilm. The poor EET likely decreased the power density. In summary, the macropores increased the loading of biomass which improved EET efficiency and MFC performance.

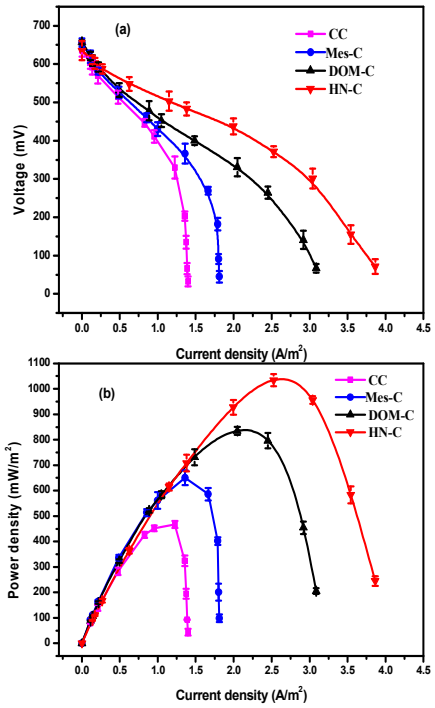

Fig.6 Voltage output curve (a) and power density outputs (b) of MFCs using different porous carbons.

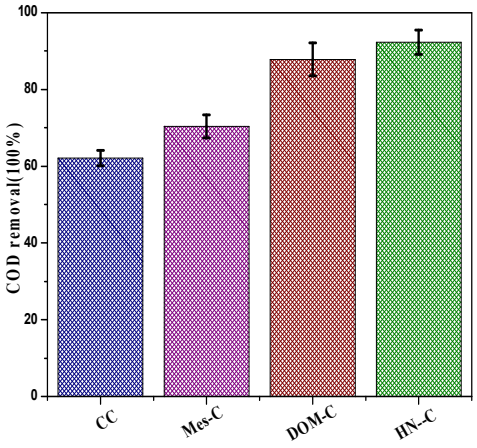

Fig. 7 COD removal rate of MFCs using different porous carbon anodes.

MFC performance on different anodes

Observed from the power polarization (Fig. 6a) and power density curves (Fig. 6b), the maximum voltage 0.56 V (Fig. S3), maximum current density 3.87 A m^{-2} and the maximum power output 1034 mW m^{-2} were observed for HN-C anode MFC. Compared with CC anode (467 mW m^{-2}), about 2.2 times of the maximum power density revealed that HN-C exhibited an excellent bioelectrochemical activity. The calculated BET specific of the Mes-C with smaller pore size (1207.0 m^2 g^{-1}) was larger than the HN-C with larger pore size (947.5 m^2 g^{-1}), but yields lower power output (811 mW m^{-2}), indicating that suitable pores size is necessary for the formation of biofilm. Though Mes-C had a higher surface area, its power production performance deteriorated due to a low biomass loading and poor electrolyte accessibility within interconnected channel structure exhibited a much higher ion-transport resistance[35]. Both of the DOM-C and HN-C possessed uniform macropores (~400nm) and similar macropore volume. However, the BET of HN-C was much larger than the DOM-C and obtained higher power output, demonstrating the surface area was important for power output. Higher bacteria loading and higher EET efficiency of the HN-C anode enabled its higher output power density than the DOM-C anode (811 mW m^{-2}) and Mes-C (678 mW m^{-2}) anode. In addition, we have evaluated the stability of the composites decorated anode, operating the MFC for one month. During this long period operation, in all cycles, the peak voltage of 0.53-0.56V was observed. The results proved that this fabricated anode could be operated for real application.

The COD removal was summarized (Fig. 7) during different mode of operation. Compared with CC anode and Mes-C anode, the COD degradation efficiency for the HN-C anode system (92.1%) was larger than the other anode systems under the same conditions, which implied that HN-C anode system was able to achieve power output without wastewater performance

deterioration. Higher COD removal at almost the same level feed COD contents due to higher biomass concentration. The COD removal of HN-C was slight higher than DOM-C (88.3%) which confirmed mesopores enhancing the transport of substrate.

The excellent performance of HN-C anode was mainly attributed to their porous structure. A high specific surface area resulted from the mesoporous structure and accessible macropores for bacterial attachment, facilitated a fast electrons transfer to HN-C anode. Furthermore, the combination of the meso- and macro- pores enhanced the transport of substrate and electrons. The particle size of the HN-C was in micrometer-size range with parts of the nanometer size range. The incorporation of macroporousity into hierarchically mesoporous carbon materials reduced diffusion lengths with the aid of macro-channels and hierarchically porous structure, resulting in a fast nutrition and ion transport. Large bacteria capacity, fast substrate transfer and electrons transfer guaranteed a larger power output for MFC.

Conclusions

This work first demonstrated the successful fabrication of 3D HN-C for a higher performance MFC (1034 mW m^{-2}), which was 2.2-folds that of CC anode. This hierarchical nanostructure carbon with mesopores and controlled macropores provided an easily accessible surface area for bacteria to adhere and facilitated fast substrate and electrons transfer. This new architectural design would overcome the poor surface area of macroporous materials in previous anode materials, and further boost anode fabrication and its MFC applications.

Acknowledgements

This work was financially supported by Natural Science Foundation of China (no. 91545126, 21328602 and 21273120), GEFC09-12, and NCET-08-0296.

Notes and references

1 B. E. Logan, B. Hamelers, R. Rozendal, U. Schrorder, J. Keller, S. Freguia, P. Aelterman, W. Verstraete and K. Rabaey, *Environ. Sci. Technol*., 2006, **40**, 5181.
2 J. Huang, N. Zhu, T. Yang, T. Zhang, P. Wu and Z. Dang, *Biosens. Bioelectron*., 2015, **72**, 332.
3 X. Chen, D. Cui, X. Wang, X. Wang and W. Li, *Biosens. Bioelectron*., 2015, **69**, 135-14.
4 C. Zhao, Wang, Y., Shi, F., Zhang, J., Zhu, J.J., 2013. Chem. Commun. 49, 6668-6670.
5 X. Xie, G. Yu, N. Liu, Z. Bao, C. S. Criddle and Y. Cui, *Energ. Environ. Sci.,* 2012, **5**, 5265.
6 P. Luo, S.J. You and J.Y. Wang, *Biosen. Bioelectron*., 2010, **25**, 1248.
7 A. Mekawy, H. Hegab, X. Dominguez-Benetton and D. Pant, *Bioresour. Technol.,* 2013, **142**, 672.
8 X. Wang, S. A. Cheng, Y.J. Feng, M.D. Merrill, T. Saito and B.E. Logan, *Environ. Sci. Technol*., 2009, **43**, 6870.
9 B.E. Logan, Microbial Fuel Cells, John Wiley and Sons, Inc., Hoboken, New Jersey, 2008, p. 63.
10 Q. Deng, X.Y. Li, J.E. Zuo, A. Ling and B.E. Logan, *J. Power Sources*, 2010, **195**, 1130.
11 H.Y. Tsai, C. C. Wu, C.Y. Lee and E.P. Shih, *J. Power Sources*, 2009, **194**, 199.
12 G. Wang, L. Zhang and J. Zhang, *Chem. Soc. Rev.* 2011, **41**, 797.
13 F.B. Su, X.S. Zhao, Y. Wang, J.H. Zeng, Z.C. Zhou and J.Y. Lee, *J. Phys. Chem. B*, 2005, **109**, 20200.
14 Y. Zhang, J. Sun, B. Hou, Y.Y. Hu, *J. Power Sources,* 2011, **196**, 7458.
15 X. Xie, L. Hu, M. Pasta, G. F. Wells, D. Kong, C. S. Criddle and Y. Cui, *Nano Lett.,* 2011, **11**, 291.
16 Y. Yuan, S.G. Zhou, Y. Liu and J.H.Tang, *Environ. Sci., Technol.* 2013, **47**, 14525.
17 Y.C. Yong, X.C. Dong, M.B. Chan-Park, H. Song and P. Chen, *ACS Nano*, 2012, **6**, 2394.
18 Z. He, J. Liu, Y. Qiao, M.C. Li and T.T. Tan, *Nano Lett*. 2012, **12**, 4738.
19 Y.J. Feng, Q.Yang, X. Wang and B.E. Logan, *J. Power Sources*, 2010, **195**, 1841.
20 M. Liu, M. Zhou, H. Yang, Y, Zhao and Y. Hu, *RSC Adv*., 2015, **5**, 84269.
21 H.Wang, Q. Gao and J. Hu, *J. Am. Chem. Soc.* 2009, **131**, 7016.
22 S. Chen, H. Hou, F. Harnisch, S. A. Patil, A. A. Carmona-Martinez, S. Agarwal, Y. Zhang, S. Sinha-Ray, A. Yarin, A. Greiner and U. Schröder, *Energ. Environ. Sci.,* 2011, **4**, 1417.
23 R. Karthikeyan, B. Wang, J. Xuan, J. W. C. Wong, P. K. H. Lee and M. K. H. Leung, *Electrochim. Acta,* 2015, **157**, 314.
24 G.H. Bogush, M.A.Tracy and C.F. Zukoski, *J. Non-Cryst. Solids.* 1988, **04**, 95.
25 L. Zhu, Y. Lu, Y. Wang, L, Zhang and W. Wang, *Appl. Surf. Sci*., 2012, **258**, 5387.
26 C.H. Huang, R.A. Doong, D. Gu and D.Y. Zhao, *Carbon*, 2011, **49**, 3055.
27 T.C. Chou, C.H. Huang, R.A. Doong and C.C,Hu, *J. Mater. Chem. A,* 2013, **1**, 2286.
28 M. Zhou, M. Chi, H. Wang and T. Jin, *Biochem. Eng. J.,* 2012, **60**, 151.
29 D.J. Kim, H.I. Lee, J.E. Yie, S.J. Kim and J.M. Kim, *Carbon*, 2005, **43**, 1868.
30 H. Liu, S. Wen, J. Wang and Y. Zhu, *J. Appl. Polym. Sci.,* 2012, **123**, 3255.
31 M. S. P. Shaffer, X. Fan and A. H. Windle, *Carbon,* 1998, **36**, 1603.
32 M. Sevilla and A.B. Fuertes, *Chem. Eur. J.,* 2009. **15**, 2117.
33 K. Guo, S. Freguia, P.G. Dennis, X. Chen, B. C. Donose, J. Keller, J. J. Gooding and K. Rabaey, *Environ. Sci. Technol.,* 2013, **47**, 7563.
34 A. Deeke, T.H. Sleutels, H.V. Hamelers and C.J. Buisman, *Environ. Sci. Technol.,* 2012. **46**, 3554.
35 Y. Zhu, S.Murali, M.D. Stoller, K.J. Ganesh, W. Cai, P. J. Ferreira, A. Pirkle, R.M. Wallace, K.A. Cychosz, M. Thommes, D. Su, E.A. Stach, and R.S. Ruoff, *Science*, 2011, **332**, 1537.
36 Z. He and F. Mansfeld, *Energ. Environ. Sci*., 2009, **2**, 215.
37 M.E. Hernandez and D.K. Newman, *Cell. Mol. Life. Sci.,* 2001, **58**, 1562.

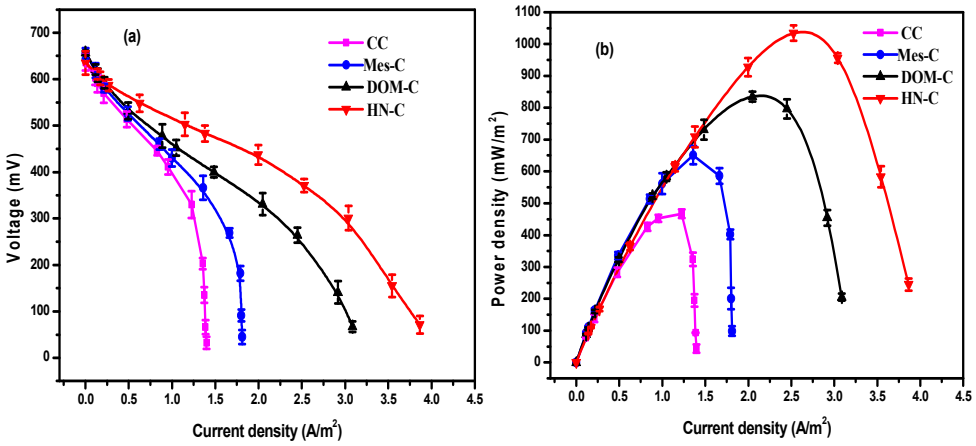

The HN-C exhibited a high power density (1034 mW m^{-2}), which was much higher than the macroporous carbon anode MFC (811 mW m^{-2}) and mesoporous carbon anode MFC (678 mW m^{-2}) and was 2.2-folds that of carbon cloth anode MFC (467 mW m^{-2}).